

## Classical Spin Chains Mimicked by Room-Temperature Polariton Condensates

Song Luo, Liming Liao, Zhe Zhang, Jun Wang, Xuechu Shen, and Zhanghai Chen<sup>\*</sup>

*State Key Laboratory of Surface Physics, Key Laboratory of Micro and Nano Photonic Structures (Ministry of Education), Department of Physics, Collaborative Innovation Center of Advanced Microstructures, Fudan University, Shanghai 200433, China and Collaborative Innovation Center of Advanced Microstructures, Nanjing University, Nanjing, Jiangsu 210093, China*



(Received 14 March 2019; revised manuscript received 11 December 2019; accepted 18 March 2020; published 21 April 2020)

A large number of optimization problems of extremely complex systems in the real world remain highly challenging for conventional digital computers. Some such problems can be mapped into the Ising model, and then efficiently solved by searching for the global minimum of the Ising Hamiltonian. Finding an appropriate physical system for efficient simulation of the Ising model is a promising way of addressing such optimization problems that has recently emerged. Here we report on the realization of analog-spin chains of exciton-polariton condensates that mimic a chain of classical spins. This is done with a room-temperature system based on a one-dimensional polariton lattice that is induced by exciting a ZnO microrod with a controllable periodic laser pattern. Depending on the lattice constant chosen, the spontaneously phase-locked condensates show either an antiphase ( $\pi$ ) or an in-phase (zero) ordering in the steady state, which mimics the antiferromagnetic or ferromagnetic state in the one-dimensional classical Ising model. In addition, when the external excitation power is increased, a chain of coupled condensate pairs, characterized by a small phase shift between the neighboring condensates that is induced by the tunneling effect, arises at a lower energy. These observations pave the way to the realization at room temperature of analog-spin simulators based on periodic condensates of exciton polaritons.

DOI: 10.1103/PhysRevApplied.13.044052

### I. INTRODUCTION

The majority of extremely complex problems in the real world, such as the dynamics of neural networks [1], protein folding [2], and portfolio optimization in financial markets [3], cannot be tackled with a classical digital computer, since their complexity grows exponentially with the dimensions of the problem. Fortunately, many such problems can be mapped into the Ising model and then solved through finding the global minimum of the Ising Hamiltonian [4,5]. The Ising model was originally proposed to study the ferromagnetic phase transition [6], but has been widely and successfully used for describing nonmagnetic phenomena such as political elections and optimization of cognitive wireless networks. Simulating the Ising Hamiltonian with the use of a specially tailored physical system is a promising approach that has recently emerged to tackling such complex problems. In recent decades, ultracold atoms in optical lattices [7], optical parametric oscillators [8,9], coupled lasers [10], superconducting circuits [11], trapped ions [12], etc. have been explored for simulating the behavior of spins governed by the Ising model. Very recently, the spontaneous buildup of a phase-locked network of bosonic

condensates of exciton polaritons (composite bosons originating from strong exciton-photon coupling [13,14]) based on two-dimensional planar microcavities has been proposed as a promising platform for simulation of the  $XY$  spin Hamiltonian [15–17]. By changing the Josephson coupling strength between the separated condensates, a phase transition in a chain of polariton condensates between antiferromagnetic (AFM) and ferromagnetic (FM) phases can be realized [18]. In the majority of experiments on multisite polariton condensates based on planar microcavities, the measurements have been performed at cryogenic temperatures; this requirement is imposed by the use of relatively low-gap semiconductor materials such as GaAs, usually grown by highly involved molecular-beam-epitaxy methods [10,15,18–20]. This greatly limits the practical application of polariton simulators. Here, we report on a development in the field of polariton Ising simulators and show a controllable AFM-FM phase transition in a chain of polariton condensates generated at room temperature.

Furthermore, we go beyond demonstrating the AFM-FM phase transition in a chain of polariton condensates and explore the rich physics of spin chains mimicked by chains of polariton condensates. One of the fascinating properties of the exciton-polariton system is a strong nonlinearity that leads to a variety of many-body effects [21,22]. We take advantage of the rich physics of a driven dissipative

\*zhanghai@fudan.edu.cn

nonlinear polariton system to search for nontrivial solutions of the Ising model such as spin-current states.

Experimentally, we nonresonantly excite a ZnO microrod with controllable laser pumping beams periodically arranged in space. Thanks to the large exciton binding energy (approximately 60 meV) and oscillator strength [23], a ZnO microrod serving as a one-dimensional (1D) whispering-gallery microcavity (WGM) provides an excellent platform for investigating strong exciton-photon coupling [24] and for generating 1D polariton condensates [25]. Here, the high-quality (with a  $Q$  factor of approximately 1600) 1D ZnO WGM is grown by a simple carbothermal reduction method, and a double-slit interferometer is employed to produce the periodic pumping beams. We experimentally and theoretically demonstrate the spontaneous buildup of a phase-locked chain of periodic polariton condensates that mimics a 1D classical spin lattice and may be employed as a 1D Ising-model simulator. In our system, the phases of the condensates are mapped to spin-up and spin-down states, and spin-spin interactions are accounted for by the phase coupling between neighboring condensates. The ground state of the Ising Hamiltonian is mimicked by polariton condensates arranged in antiphase or in phase, which correspond to an AFM or FM spin state. Interestingly, with an increase in the external excitation power, the enhanced nonlinear interaction between quasi-particles breaks the equilibrium of the Ising-like chain and induces a system of paired condensates that is characterized by a different spatial distribution of condensates and their periodicity. Meanwhile, a type of analog-spin chain of paired condensates is observed due to tunneling-based phase correlations between the condensates. The effective potential, which is formed due to an enhanced nonlinearity triggered by a higher pumping density, provides a mechanism for coupling of the condensates through the tunneling effect, which leads to the formation of a phase characterized by a small relative phase difference between paired condensates, and thus forms an analog-spin order equivalent to a superfluid polariton-flow state.

## II. RESULTS

### A. Polariton lattice

As mentioned above, in order to create a polariton lattice, a simple double-slit interferometer is used to produce periodic laser beams for pumping the 1D ZnO WGM. As shown in Fig. 1(a), the periodic excitation beams are produced when a nanosecond pulsed(20 kHz) laser beam crosses the double-slit and interferes with itself. Here, an objective ( $15\times$ ) is used to focus the beams. The real-space image of these beams taken from the focal plane of the objective in Fig. 1(b) shows the layout of the excitation laser spots. The black line shows the intensity profile. A sine-squared function is employed to fit the data (red line). The period  $a$  of the excitation beams, which is also the

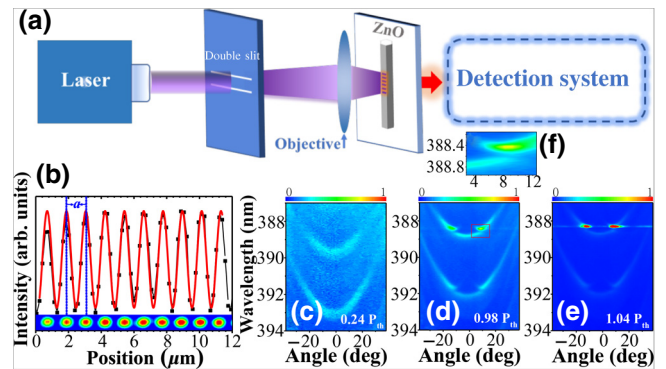


FIG. 1. Formation of a 1D polariton lattice. (a) Schematic illustration of the experimental setup for creating periodic excitation beams. (b) Periodic excitation beams created by double-slit interference of a 355-nm nanosecond pulsed laser beam; the inset image at the bottom is a real-space image of the excitation beams taken from the focal plane of the excitation objective. The black line shows the profile of the excitation beams, and the red line shows a fit of the data made with the use of a sine-squared function. (c)–(e) Angle-resolved PL spectra taken with different average pump powers: (c) 0.24, (d) 0.98, and (e) 1.04 times threshold. Here, the lattice constant  $a$  is  $1.3\ \mu\text{m}$ . (f) Enlarged region identified by the red rectangle in (d). The polariton gap in (f) is approximately 2.1 meV.

laser-induced polaritonic lattice constant, can be continuously changed by varying the spacing of the double slit or the distance between the double slit and the objective, while the size of the excitation spots remains almost unchanged. The angle-resolved photoluminescence (PL) spectra in Figs. 1(c)–1(e) show the evolution of the band structure of the polariton lattice with increasing pumping power. In this case ( $a = 1.3\ \mu\text{m}$ ), only the two lower polariton branches are taken into consideration. When the pumping power is increased, the band structure shows a striking variation. At low pumping power, the spectrum in Fig. 1(c) exhibits the parabolic-like dispersion of polaritons in a ZnO WGM. However, when the pumping power approaches a threshold, an avoided crossing of the polariton branches appears, resulting in distinct band gaps at the edge of the first Brillouin zone, which demonstrate the formation of a polariton lattice [see Fig. 1(d)]. The enlarged region identified by the red rectangle in (d) shows an opening gap (approximately 2.1 meV) at  $k_{\parallel} = \pi/a$ , as shown in Fig. 1(f). These effects are caused by the modulation of the periodic potential induced by the pumping laser as well as the strong polariton-polariton and polariton-reservoir interactions. At higher densities of polaritons and in the presence of a hot-exciton reservoir, the average momentum of exciton polaritons in the direction along the ZnO microwire axis increases due to their repulsive interactions [19]. Interestingly, once the pump power exceeds the threshold, the system spontaneously builds up an antiphase ( $\pi$ -state) condensate located at the

edge of the first Brillouin zone. This is similar to the results of a low-temperature experiment performed on a GaAs-based microcavity [26].

### B. Ising chain of polariton condensates

Time-integrated spatially resolved PL spectra showing periodic polariton condensates in real space, whose lattice constant increases from 1.3 to 6.4  $\mu\text{m}$ , are shown at the bottom of each panel in Fig. 2. Degenerate macroscopic coherent multiple condensates form at each excitation site at the threshold. The coherence of the condensates can be demonstrated through interferometry or Fourier-space analysis (see the angle-resolved PL spectra in Fig. 4). Away from the pump spots, distinguishable standing waves (fringes) between neighboring condensates can be clearly seen. This is the result of interference of coherent polaritons emitted from neighboring sites due to the repulsive polariton-exciton and polariton-polariton interactions within each condensate. Such an interference effect not only demonstrates the coherence of the polariton condensates at each pumping site but also provides a channel for phase coupling between the condensates. Just as in the case of the interference of electromagnetic waves emitted by pointlike sources, the number of interference fringes determines the phase difference between the neighboring condensates in our system. Consequently, the phase difference between neighboring condensates can be deduced from the number of fringes formed: it is zero or even for the antiphase configuration, and odd for the in-phase configuration. Moreover, through analysis of the

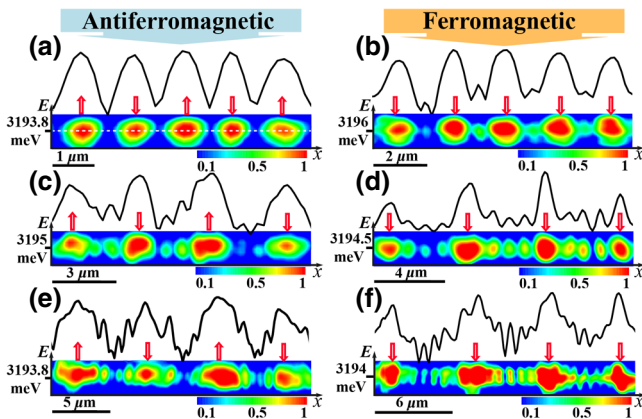


FIG. 2. Ising chains of 1D polariton condensates. The left (right) panel corresponds to a phase-locked AFM (FM) chain of condensates. The lattice constant from (a) to (f) is 1.3, 2, 3.1, 4.3, 5.3, and 6.4  $\mu\text{m}$ , respectively. The black curves correspond to the intensity profile of the chain of condensates as marked by the white dotted line at the bottom of Fig. 2(a), and the same line applies to (b)–(f). Here, the phase of each condensate is mapped to up or down spin states, shown by the red arrows. The antiparallel and parallel arrangements correspond to the AFM and FM states, respectively.

corresponding Fourier-space spectra, the relative phase difference between condensates can also be known (see Fig. 4). For coupled condensates, a zero or even number of fringes reveals a relative phase difference of  $\pi$  between the nearest-neighbor sites, and a odd number of fringes reveals a relative phase difference of zero, which mimics AFM and FM coupling, respectively, in the Ising model.

In such a periodic excitation configuration, we observe that the threshold for polariton condensation is sensitive to the relative phase between the condensates. The phase-locked  $\pi$  or zero steady states that have the lowest threshold will first populate the ground state of the 1D Ising Hamiltonian  $H = -\sum_{ij} J_{ij} s_i s_j$ , where  $s_i$  is the  $i$ th spin value ( $s_i \in \{-1, 1\}$ ),  $J_{ij}$  is the strength of the interaction between the spins  $s_i$  and  $s_j$ , and  $s_i s_j = \cos(|\theta_j - \theta_i|)$ . In order to simulate the Ising model effectively with our system, coupling elements that have a binary degree of freedom are required. Here, the phases  $\theta_i$  of the condensates are mapped into the 1D Ising model, and only the nearest-neighbor interactions between the “spins” are taken into consideration (namely, for the distance between nearest neighbors  $d_{ij} = a$ ). For a 1D chain, the phase coupling  $J_{ij}$ , which depends on the distance  $d_{ij}$ , the out-flowing momentum  $k_x$  and the density  $|\psi(k)|^2$  [15,17,27] are linked by

$$J_{ij} = \frac{2}{\pi} \int_0^\infty |\psi(k)|^2 \cos(k_x d_{ij}) dk, \quad (1)$$

where  $\psi(k)$  is the wave function in  $k$ -space, and  $|\psi(k)|^2 \sim \delta(k - k_x)$  [17]. Positive and negative  $J_{ij}$  represent coupling constants characteristic of FM and AFM spin arrangements, respectively. By changing the period of the excitation beams to control  $d_{ij}$  and  $k_x$  (see Figs. 2 and 4), one can invert the sign of  $\cos(k_x d_{ij})$  and also  $J_{ij}$ , which leads to a transition between the AFM and FM states. Obviously, the final phase-locked  $\pi$  or zero steady condensation state that is driven by the bosonic stimulation has the maximum polariton occupation number [27]. If  $J_{ij}$  is positive (negative), this indicates that the system will spontaneously lock into an in-phase (antiphase) state between nearest neighbors, so that  $\cos(|\theta_i - \theta_{i-1}|) = 1$  ( $-1$ ), and thus the energy of the effective spin system is minimized. As the polariton density increases with an increase in the pumping power, the coupling strength becomes stronger. The polaritons thus spontaneously condense into the antiphase (left panels in Fig. 2) or in-phase (right panels in Fig. 2) state when the average pumping power reaches a threshold. For the 1D classical Ising model, the ground state of the Hamiltonian corresponds to the FM (AFM) state, in which the spins are arranged in a parallel (antiparallel) configuration and the spin at each site can occur only in the spin-up or spin-down state. The observed relative phase difference between neighboring condensates in our system appears to be shown to be either zero or  $\pi$ , which mimics either FM or AFM

solutions, respectively, of the Ising model. As analyzed above, by mapping the phase of each polariton condensate to the spin-up or spin-down state, the ground state of the Ising Hamiltonian can be simulated by simply observing the steady state of the spontaneously coupled condensates. This result indicates that some non-deterministic polynomial complete (NP-complete) problems relevant to finding the global minimum of an associated cost function can be efficiently solved by mapping them to our system.

To describe the behavior of the chain of coupled periodic polariton condensates and verify the type of phase coupling analyzed above, we employ the phenomenological complex Ginzburg-Landau equation [15,28] to model the system:

$$\begin{aligned} i\hbar \frac{\partial \psi_x}{\partial t} = & \left[ \frac{-\hbar^2}{2m} \nabla^2 + g_p |\psi_x|^2 + \hbar g_R N_R(x) + V(x) \right] \psi_x \\ & + \frac{i\hbar}{2} (\eta N_R(x) - \Upsilon_p) \psi_x, \end{aligned} \quad (2)$$

$$\frac{\partial N_R}{\partial t} = -\eta N_R(x) |\psi_x|^2 + \rho P(x). \quad (3)$$

Here,  $m$  is the effective mass of the polariton;  $g_p > 0$  and  $g_R > 0$  characterize the strength of the polariton-polariton and polariton-reservoir interactions, respectively (both of these interactions lead to a blueshift of the polariton condensate and also formation of an effective potential for the polaritons);  $N_R(x)$  is the density of the hot-exciton reservoir;  $V(x) = \xi P(x)$  is the effective potential induced by the periodic excitation beams;  $\xi$  is a constant coefficient;  $P(x) = A \sin^2(\pi x/\omega)$  is the profile of the effective excitation beams, as shown in Fig. 1(b) ( $A$  is the amplitude);  $\eta$  is the relaxation rate at which the exciton reservoir feeds the polariton condensates;  $\Upsilon_p$  is the decay rate of the condensed polaritons; and  $\rho P(x)$  describes the pumping into the exciton reservoir.

Figure 3 shows the time-integrated results of a numerical simulation using the Ginzburg-Landau equation, assuming values of the lattice constant taken from the experimental results in Fig. 2. These steady-state solutions reproduce well the chain of condensates and the corresponding phase configurations demonstrated experimentally in Fig. 2. The black curve in Fig. 3(a) corresponds to the intensity profile of the chain of condensates marked by the white dotted line at the bottom, and this applies also to Figs. 3(b)–3(f). We extract the relative phases of the condensate wave functions as shown by the blue curves. We clearly see that the relative phase difference of the nearest-neighbor condensates switches between zero and  $\pi$  as the lattice constant increases. Owing to the nonlinear repulsive interaction and the coherence of the condensates, there are interference fringes formed between the nearest-neighbor condensates. Consequently, the type of phase coupling can

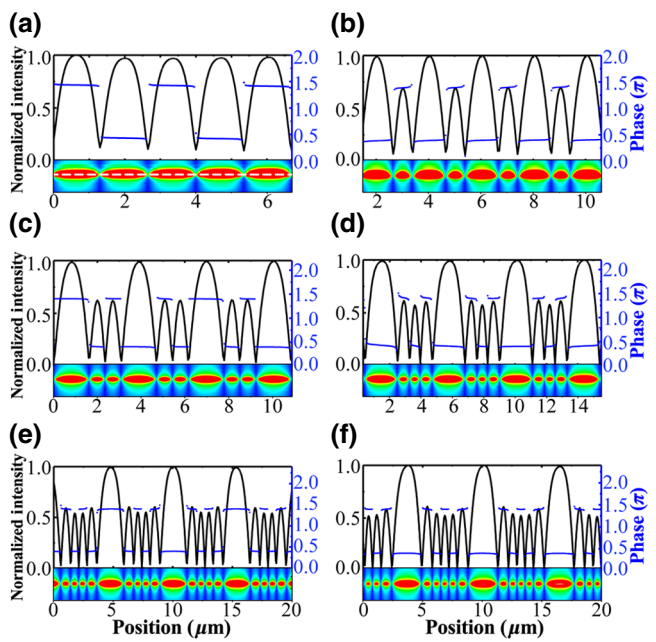


FIG. 3. Results of theoretical modeling of an Ising chain of polariton condensates in different phase configurations. The spontaneous buildup of polariton condensates results in the formation of phase-locked AFM (left panel) and FM (right panel) steady states, as these simulations show. The lattice constant from (a) to (f) is 1.3, 2, 3.1, 4.3, 5.3, and 6.4  $\mu\text{m}$ , respectively.

be deduced from the number of fringes (which indicate a standing wave): zero or even for the AFM coupling (left panels in Fig. 3), and odd for the FM coupling (right panels in Fig. 3).

For the periodic chain of polariton condensates in our experiment, the phase difference between condensates can also be verified by a Fourier-space analysis. The experimental data in Fig. 4 show angle-resolved (Fourier-space) PL spectra taken from the polariton Ising chain shown in Fig. 2. By changing the lattice constant, one can switch the polariton condensation state between antiphase  $\pi$  states [(a), (c), and (e) in Fig. 4] and in-phase zero states [(b), (d), and (f) in Fig. 4]. Here, for the zero states the wave vector is  $k_{\parallel} = \pm 2n\pi/a$  ( $n = 0, 1, 2, \dots$ ); for the  $\pi$  states, the wave vector is  $k_{\parallel} = \pm (2n+1)\pi/a$  ( $n = 0, 1, 2, \dots$ ). As one can see in Fig. 4(a), the system spontaneously builds up a  $\pi$ -state polariton condensate at the edge of the first Brillouin zone, similar to that observed by Lai *et al.* in a GaAs system [26]. For the  $\pi$  state (zero state), the wave function in real space exhibits a difference of  $\pi$  (zero) between adjacent condensates. The occurrence of destructive or constructive interference at the position of zero momentum in Fourier space depends on the relative phase difference between the condensates in real space. Namely, if the phase difference is  $\pi$  (zero), destructive (constructive) interference will be established at the position of zero momentum. Fourier-space time-integrated

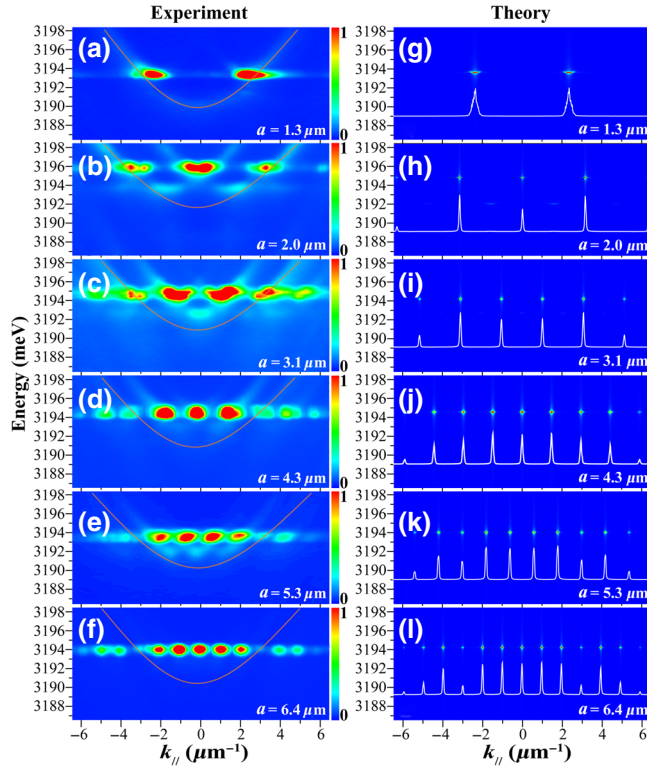


FIG. 4. Fourier-space PL images of a 1D polariton Ising chain in the configurations corresponding to Fig. 2. The left panels show the experimental data, and the right panels show the results of theoretical calculations. The red guide line in each left panel corresponds to the polariton eigenmode of a 1D WGM. The momentum of the condensates in the polariton eigenmode marked by the red guide line corresponds to  $k_x$  in our paper. The white curves in each right panel are profiles of degenerate polariton condensates with different momenta.

images obtained by a numerical simulation are shown in the right panels in Fig. 4. This simulation reproduces well the experimental results.

### C. Analog-spin order

Naturally, the equilibrium of the chain of periodic condensates (AM or AFM) will be broken if the external conditions, e.g., the pumping power, are changed. It can be expected that condensates with other phase configurations may form when the pumping power increases beyond the threshold for the FM or AFM state. Effectively, as one can see in Figs. 5(a)–5(d), in this regime the polaritons condense at the two sides of each potential at lower energy. We shall refer to this state as a state of periodic pair condensates. Figures 5(c) and 5(d) are schematic illustrations of the dynamics of the formation of the pair condensates shown in Figs. 5(a) and 5(b). We attribute the splitting of each original condensate into a pair to polariton-polariton and polariton-reservoir interactions, as well as to an acoustic-phonon scattering effect.

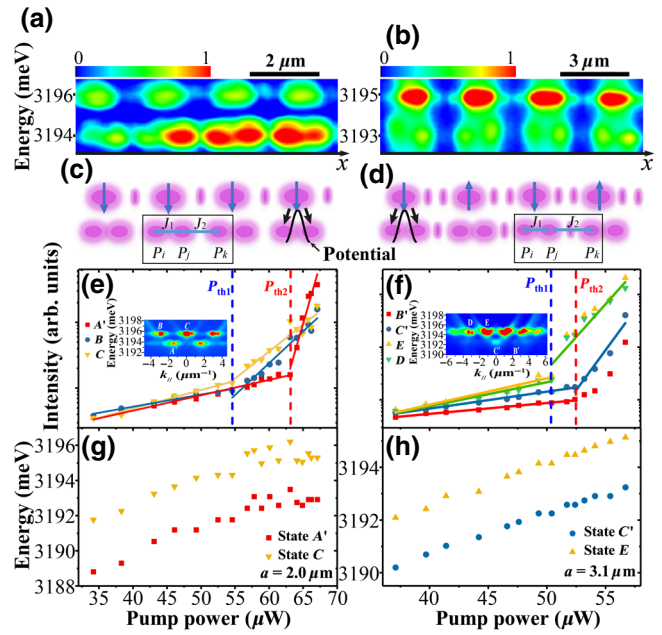


FIG. 5. Formation of pairs of condensates arranged in new phase configurations. (a),(b) PL mapping in real space above the threshold  $P_{\text{th}2}$ ; the lattice constant is 2.0 and 3.1  $\mu\text{m}$ , respectively. (c),(d) Schematic illustrations of the dynamics of systems corresponding to the experimental images in (a),(b), respectively. (e),(f) Integrated intensity of individual condensates as a function of average pump power. The insets show Fourier-space images, indicating condensates corresponding to the data in terms of the pump power. (g),(h) Blueshifts of the energies of the same states as in (e),(f) as functions of the pump power.

At higher excitation power, above the first threshold  $P_{\text{th}1}$  [shown in Figs. 5(e) and 5(f)], the acoustic-phonon scattering effect cannot be neglected, due to the heating effect of the laser, and it leads directly to relaxation of the polaritons to a lower-energy state through phonon emission [29,30]. Meanwhile, thanks to the nonlinear effects triggered by the exciton component, the repulsive interaction between the exciton reservoir and the polaritons and the polariton-polariton repulsion become stronger with an increase in the pump intensity. As a result, part of each condensate is split into two parts, and the newly formed condensates are repelled to the two sides of the effective potential in real space. The dependence of the energy blueshift on the pump power intensity shown in Figs. 5(g) and 5(h) proves that the nonlinear interactions in the system become stronger with an increase in the pump power. The insets in Figs. 5(e) and 5(f) show Fourier-space images corresponding to Figs. 5(a) and 5(b), respectively. The corresponding dependence on the pump power, exhibiting two thresholds for condensation in Figs. 5(e) and 5(f), reflects the typical dynamics of the formation of the pair condensates. The polaritons first condense into a ferromagneticlike or antiferromagneticlike state at the threshold  $P_{\text{th}1}$ .

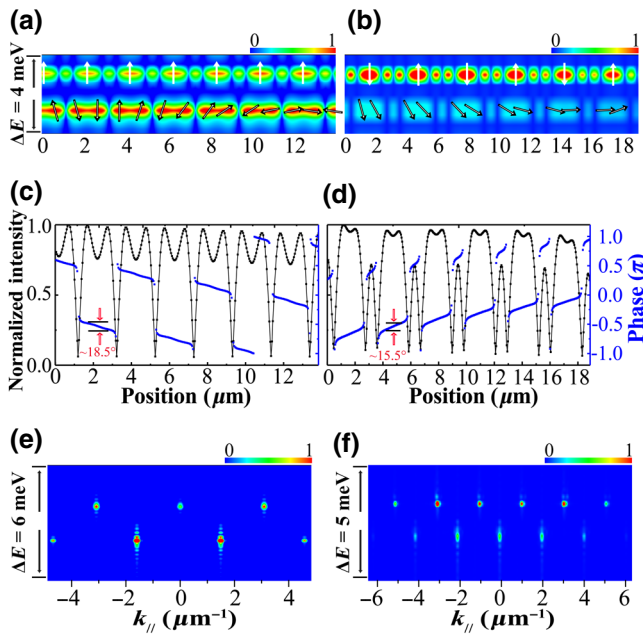


FIG. 6. Results of numerical simulation: two distinguishable effective spin chains at two different energies formed in the same real space. One is an AFM/FM chain (shown by the white arrows), and the other is an exotic analog-spin chain exhibiting a persistent current of exciton polaritons proportional to the phase gradient (shown by black arrows). (a),(b) Distribution of steady states of the condensates in the polariton lattice. Here, the lattice constants, i.e., the periods of the effective potential, are 2.0 and 3.1  $\mu\text{m}$ , taken from the experiments in Fig. 5. The effective spins shown by the arrows are oriented according to the relative phases of the condensates shown in (c),(d). The phase differences between the paired condensates in (a),(b) are approximately  $18.5^\circ$  and  $18.5^\circ$ , respectively. Meanwhile, the phase differences between  $P_j$  and  $P_k$  (illustrated in Fig. 5) are  $\pi$  in (a) and 0 in (b), which is why the directions of the corresponding arrows are antiparallel in (a) and parallel in (b). (c),(d) Density profile and corresponding phase configuration of the periodic paired condensates in the lower-energy state in (a),(b). (e),(f)  $k$ -space images corresponding to the real-space images in (a),(b).

and then relax in energy, sliding down along the effective potential [shown by the black curves in Figs. 5(c) and 5(d)] and eventually condensing into a lower-energy state at  $P_{\text{th}2}$ . In the latter case, an effective potential barrier separates the paired condensates  $P_i$  and  $P_j$ , as marked in Figs. 5(c) and 5(d), and therefore a phase-coupling mechanism based on the tunneling effect is realized [18]. For this state of periodic pair condensates, two different phase-coupling mechanisms govern the phase locking for condensates belonging to the same pair or different pairs. Thus the effective spin Hamiltonian takes the form  $H = -J_1 \sum_{ij} s_i s_j - J_2 \sum_{jk} s_j s_k$ , where  $J_1$  and  $J_2$  are the coupling strengths corresponding to tunneling-based coupling and coupling due to the exchange of ballistically propagating polaritons, respectively.

The phase difference between  $P_j$  and  $P_k$  [marked in Figs. 5(c) and 5(d)] is easily deduced from the number of interference fringes. However, it is still ambiguous for the paired condensates ( $P_i$  and  $P_j$ ). Through the relaxation process mentioned above, the polaritons condense into a certain state, i.e., paired condensates, which are governed by the period and the relative intensity of the effective potential in a polariton lattice. Therefore, in the absence of the energy-relaxation process in Eqs. (2) and (3), one can directly obtain the steady-state distribution of the paired condensates in the chain and find the corresponding phase configuration by a numerical simulation assuming a specific effective periodic potential (see the Appendix). The numerical results presented in Fig. 6 show the steady-state distribution of the polariton density and phase at two distinguishable energy levels. The calculation results agree well with the experimental data shown in Fig. 5. Figures 6(c) and 6(d) show the density profile (black curve) and the phase configuration (blue dots) of the corresponding lower-energy periodic paired condensates shown in Figs. 6(a) and 6(b), respectively. The tunneling-based coupling allows a small relative phase difference between the paired condensates. As a result, the phases of the condensates exhibit a type of “order” in which the orientation of the effective spins changes gradually along the chain [shown by the black arrows in Figs. 6(a) and 6(b)]. The spontaneous formation of a phase gradient in a chain of polariton condensates is indicative of spontaneous symmetry breaking, leading to the appearance of a persistent superfluid current of polaritons in the direction defined by the sign of the phase gradient. Such current states in periodic arrays of polariton condensates have been theoretically predicted in Ref. [31] but have remained experimentally elusive. In terms of the effective spins, this current state may be characterized as a spin wave. The  $k$ -space images shown in Figs. 6(e) and 6(f) are obtained by taking the Fourier transform of the real-space wave functions shown in Figs. 6(a) and 6(b). The numerical results agree well with the experimental data shown in Fig. 5.

### III. CONCLUSION

In summary, we create an optically controlled 1D analog-spin chain based on a lattice of polariton condensates at room temperature. Here, the relative spin-spin orientations are mapped to the relative phases of phase-locked polariton condensates. By varying the lattice constant in the optically generated chain of polariton condensates, we show that the AFM and FM solutions of the Ising model can be effectively simulated by the system, which arranges neighboring condensates in antiphase locked and in-phase locked states, respectively. By increasing the pumping density, we achieve an exotic state where an alternative effective spin order is formed spontaneously at a lower energy due to the enhanced nonlinear interaction among

quasiparticles. This observation indicates the high potential of a 1D polariton condensate chain as an ultrafast optically controlled Ising-model simulator and also suggests its capability for predicting classical spin phases. We conclude that our system provides a promising platform for finding the global minimum of the Ising Hamiltonian, which means that some optimization problems belonging to the NP-complete class can be efficiently solved by mapping them to our system. We believe that these results pave the way to the realization of feasible ultrafast simulators based on condensates of exciton polaritons. Further steps may include the integration of Ising simulators based on ZnO nanorods into a circuit.

## ACKNOWLEDGMENTS

The work is supported by the National Key R&D Program of China (Grants No. 2018YFA0306304) and the National Natural Science Foundation of China (Grant No. 91950201 and 11674069). The authors are grateful to A. V. Kavokin, Wei Xie, and Liaoxin Sun for fruitful discussions and proofreading.

## APPENDIX

### 1. Sample fabrication

The ZnO microrod used in our experiment is fabricated by a simple carbothermal reduction method: powdered carbon and ZnO are mixed in equal proportions and then reacted at 1100°C in a constant-temperature tube furnace for 10 min, and then cooled naturally to room temperature.

### 2. Optical measurements

The PL collection for both real- and Fourier-space imaging of the polariton lattice is carried out with a home-built confocal microscope with an objective (40  $\times$ ) with a numerical aperture of 0.75. All the collected signals are TE-polarization selected by a linear polarizer, selecting the polarization perpendicular to the ZnO microrod, and then detected by a Princeton Instruments spectrometer with a cooled charge-coupled camera for time-integrated measurements.

### 3. Numerical simulation

To support our experimental results, numerical simulation of the condensation kinetics under nonresonant optical excitation is performed using the phenomenological complex Ginzburg-Landau equation [Eqs. (2) and (3)]. For each lattice constant in Fig. 3, we start with random noise as the initial values of the wave function  $\psi_x$  to find the ground-state configurations through iteration. The values of the parameters used in the numerical simulation are as follows:  $m = 1.36 \times 10^{-5} m_e$ , where  $m_e$  is the effective mass of the electron;  $g_p = 4.4 \text{ meV } (\mu\text{m})^2$ ;  $g_R = 0.05 \text{ meV } (\mu\text{m})^2$ ;  $\eta = 0.01 \text{ (ps)}^{-1} (\mu\text{m})^2$ ;  $\Upsilon_p = 0.5 \text{ (ps)}^{-1}$ ; and  $\xi/\hbar = 0.5 \text{ } (\mu\text{m})^2$ .

To obtain the steady-state polariton density and phase distribution shown in Fig. 6, we assume  $\partial N_R / \partial t = 0$ . In this way, the problem is reduced to finding the eigenstates of an effective Hamiltonian  $H = (-\hbar^2/2m)\nabla^2 + V_{\text{eff}}$ , where the effective potential  $V_{\text{eff}} = g_p|\psi_{0x}|^2 + \hbar g_R N_{0R} + V_0(x) = A \sin^2(\pi x/\omega)$  has the same shape as the potential induced by the external pumping  $V_0(x)$ , here  $g_p|\psi_{0x}|^2$ , and  $\hbar g_R N_{0R}(x) \ll V_0(x)$ .

- [1] R. Rojas, *Neural Networks-A Systematic Introduction* (Springer-Verlag, New York, 1996).
- [2] N. A. Pierce and E. Winfree, Protein design is NP-hard, *Protein Eng.* **15**, 779 (2002).
- [3] M. Hayashi, M. Yamaoka, C. Yoshimura, T. Okuyama, H. Aoki, and H. Mizuno, Accelerator chip for ground-state searches of Ising model with asynchronous random pulse distribution, *Int. J. Netw. Comput.* **6**, 195 (2016).
- [4] F. Barahona, On the computational complexity of Ising spin glass models, *J. Phys. A: Math. Gen.* **15**, 3241 (1982).
- [5] G. De las Cuevas and T. S. Cubitt, Simple universal models capture all classical spin physics, *Science* **351**, 1180 (2016).
- [6] H. Nishimori and G. Ortiz, *Elements of Phase Transitions and Critical Phenomena* (OUP Oxford, London, 2010).
- [7] J. Simon, W. S. Bakr, R. Ma, M. E. Tai, P. M. Preiss, and M. Greiner, Quantum simulation of antiferromagnetic spin chains in an optical lattice, *Nature* **472**, 307 (2011).
- [8] T. Inagaki, K. Inaba, R. Hamery, K. Inoue, Y. Yamamoto, and H. Takesue, Large-scale Ising spin network based on degenerate optical parametric oscillators, *Nat. Photonics* **10**, 415 (2016).
- [9] A. Marandi, Z. Wang, K. Takata, R. L. Byer, and Y. Yamamoto, Network of time-multiplexed optical parametric oscillators as a coherent Ising machine, *Nat. Photonics* **8**, 937 (2014).
- [10] M. Nixon, E. Ronen, A. A. Friesem, and N. Davidson, Observing Geometric Frustration with Thousands of Coupled Lasers, *Phys. Rev. Lett.* **110**, 184102 (2013).
- [11] M. W. Johnson, M. H. Amin, S. Gildert, T. Lanting, F. Hamze, N. Dickson, and E. M. Chapple, Quantum annealing with manufactured spins, *Nature* **473**, 194 (2011).
- [12] K. Kim, M. S. Chang, S. Korenblit, R. Islam, E. E. Edwards, J. K. Freericks, and C. Monroe, Quantum simulation of frustrated Ising spins with trapped ions, *Nature* **465**, 590 (2010).
- [13] C. Weisbuch, M. Nishioka, A. Ishikawa, and Y. Arakawa, Observation of the Coupled Exciton-Photon Mode Splitting in a Semiconductor Quantum Microcavity, *Phys. Rev. Lett.* **69**, 3314 (1992).
- [14] H. Deng, G. Weihs, C. Santori, J. Bloch, and Y. Yamamoto, Condensation of semiconductor microcavity exciton polaritons, *Science* **298**, 199 (2002).

- [15] N. G. Berloff, M. Silva, K. Kalinin, A. Askopoulos, J. D. Töpfer, P. Cilibrizzi, and P. G. Lagoudakis, Realizing the classical XY Hamiltonian in polariton simulators, *Nat. Mater.* **16**, 1120 (2017).
- [16] H. Sigurdsson, A. J. Ramsay, H. Ohadi, Y. G. Rubo, T. C. H. Liew, J. J. Baumberg, and I. A. Shelykh, Driven-dissipative spin chain model based on exciton-polariton condensates, *Phys. Rev. B* **96**, 155403 (2017).
- [17] K. P. Kalinin, P. G. Lagoudakis, and N. G. Berloff, Exotic states of matter with polariton chains, *Phys. Rev. B* **97**, 161101 (2018).
- [18] H. Ohadi, A. J. Ramsay, H. Sigurdsson, Y. D. V. I. Redondo, S. I. Tsintzos, Z. Hatzopoulos, and J. J. Baumberg, Spin Order and Phase Transitions in Chains of Polariton Condensates, *Phys. Rev. Lett.* **119**, 067401 (2017).
- [19] G. Tosi, G. Christmann, N. G. Berloff, P. Tsotsis, T. Gao, Z. Hatzopoulos, and J. J. Baumberg, Geometrically locked vortex lattices in semiconductor quantum fluids, *Nat. Commun.* **3**, 1243 (2012).
- [20] H. Ohadi, Y. D. V. I. Redondo, A. Dreismann, Y. G. Rubo, F. Pinsker, S. I. Tsintzos, and J. J. Baumberg, Tunable Magnetic Alignment Between Trapped Exciton-Polariton Condensates, *Phys. Rev. Lett.* **116**, 106403 (2016).
- [21] E. Wertz, L. Ferrier, D. D. Solnyshkov, R. Johne, D. Sanvitto, A. Lemaître, and G. Malpuech, Spontaneous formation and optical manipulation of extended polariton condensates, *Nat. Phys.* **6**, 860 (2010).
- [22] W. Xie, H. Dong, S. Zhang, L. Sun, W. Zhou, Y. Ling, and Z. Chen, Room-Temperature Polariton Parametric Scattering Driven by a One-Dimensional Polariton Condensate, *Phys. Rev. Lett.* **108**, 166401 (2012).
- [23] M. Zamfirescu, A. Kavokin, B. Gil, G. Malpuech, and M. Kaliteevski, ZnO as a material mostly adapted for the realization of room-temperature polariton lasers, *Phys. Rev. B* **65**, 161205 (2002).
- [24] L. Sun, Z. Chen, Q. Ren, K. Yu, L. Bai, W. Zhou, H. Xiong, Z. Q. Zhu, X. Shen, and Z. Chen, Direct Observation of Whispering Gallery Mode Polaritons and their Dispersion in a ZnO Tapered Microcavity, *Phys. Rev. Lett.* **100**, 156403 (2008).
- [25] L. Zhang, W. Xie, J. Wang, A. Poddubny, J. Lu, Y. Wang, Y. G. Rubo, and Z. Chen, Weak lasing in one-dimensional polariton superlattices, *Proc. Natl. Acad. Sci.* **112**, 201502666 (2015).
- [26] C. W. Lai, N. Y. Kim, S. Utsunomiya, G. Roumpos, H. Deng, M. D. Fraser, and Y. Yamamoto, Coherent zero-state and -state in an exciton-polariton condensate array, *Nature* **450**, 529 (2007).
- [27] H. Ohadi, R. L. Gregory, T. Freegarde, Y. G. Rubo, A. V. Kavokin, N. G. Berloff, and P. G. Lagoudakis, Nontrivial Phase Coupling in Polariton Multiplets, *Phys. Rev. X* **6**, 031032 (2016).
- [28] M. Wouters and I. Carusotto, Excitations in a Nonequilibrium Bose-Einstein Condensate of Exciton Polaritons, *Phys. Rev. Lett.* **99**, 140402 (2007).
- [29] I. G. Savenko, T. C. H. Liew, and I. A. Shelykh, Stochastic Gross-Pitaevskii Equation for the Dynamical Thermalization of Bose-Einstein Condensates, *Phys. Rev. Lett.* **110**, 127402 (2013).
- [30] K. Winkler, O. A. Egorov, I. G. Savenko, X. Ma, E. Estrecho, T. Gao, and S. Höfling, Collective state transitions of exciton-polaritons loaded into a periodic potential, *Phys. Rev. B* **93**, 121303 (2016).
- [31] A. V. Nalitov, T. C. H. Liew, A. V. Kavokin, B. L. Altshuler, and Y. G. Rubo, Spontaneous Polariton Currents in Periodic Lateral Chains, *Phys. Rev. Lett.* **119**, 067406 (2017).